4-1-2012

SRRs Embedded with MEMS Cantilevers to Enable Electrostatic Tuning of the Resonant Frequency

E. A. Moore
Air Force Institute of Technology

Derrick Langley
Air Force Institute of Technology

Matthew E. Jussaume
Air Force Research Laboratory

L. A. Rederis
Air Force Institute of Technology

C. A. Lundell
Air Force Institute of Technology

See next page for additional authors

Accepted version. *Experimental Mechanics*, Vol. 52, No. 4 (April 2012): 395-403. DOI.
Ronald A. Coutu, Jr. was affiliated with Air Force Institute of Technology at the time of publication.

Authors
E. A. Moore, Derrick Langley, Matthew E. Jussaume, L. A. Rederis, C. A. Lundell, Ronald A. Coutu Jr., Peter J. Collins, and Lavern A. Starman

Experimental Mechanics, Vol. 52, No. 4, (April, 2012): 395-403. DOI.

Contents

SRRs Embedded with MEMS Cantilevers to Enable Electrostatic Tuning of the Resonant Frequency

E. A. Moore
Air Force Institute of Technology, Wright-Patterson AFB, OH
D. Langley
Air Force Institute of Technology, Wright-Patterson AFB, OH
M. E. Jussaume
Air Force Institute of Technology, Wright-Patterson AFB, OH
L. A. Rederus
Air Force Institute of Technology, Wright-Patterson AFB, OH
C. A. Lundell
Air Force Institute of Technology, Wright-Patterson AFB, OH
R. A. Coutu Jr.
Air Force Institute of Technology, Wright-Patterson AFB, OH
P. J. Collins
Air Force Institute of Technology, Wright-Patterson AFB, OH
L. A. Starman
Air Force Institute of Technology, Wright-Patterson AFB, OH

Abstract

A microelectromechanical systems (MEMS) cantilever array was monolithically fabricated in the gap region of a split ring resonator (SRR) to enable electrostatic tuning of the resonant frequency. The design consisted of two concentric SRRs each with a set of cantilevers extending across the split region. The cantilever array consisted of five beams that varied in length from 300 to 400 μm, with each beam adding about 2 pF to the capacitance as it actuated. The entire structure was fabricated monolithically to reduce its size and minimize losses from externally wire bonded components. The beams actuate one at a time, longest to shortest with an applied voltage ranging from 30–60 V. The MEMS embedded SRRs displayed dual resonant frequencies at 7.3 and 14.2 GHz or 8.4 and 13.5 GHz depending on the design details. As the beams on the inner SRR actuated the 14.2 GHz resonance displayed tuning, while the cantilevers on the outer SRR tuned the 8.4 GHz resonance. The 14.2 GHz resonant frequency shifts 1.6 GHz to 12.6 GHz as all the cantilevers pulled-in. Only the first two beams on the outer cantilever array pulled-in, tuning the resonant frequency 0.4 GHz from 8.4 to 8.0 GHz.

Keywords
Split ring resonator; MEMS; Metamaterials; Cantilever; SRR; Microelectromechanical systems; Varactors

Introduction
Metamaterials have recently found themselves in the spotlight of materials research due to their purported ability to bypass many of the limitations of traditional materials. Metamaterials are engineered materials with electromagnetic properties tailored to have an effective negative permeability and/or permittivity when interacting with specific wavelengths of incident radiation. Metamaterials provide new prospects in the design of optical and electromagnetic devices and also suggest the fabrication of unique applications such as the perfect lens or invisibility cloak.[1,2]

Materials with negative permeability and permittivity were first investigated by Veselago in 1968.[3] He referred to them as left handed materials due to their backward interaction with electric and magnetic fields. Veselago put forth a frame work for metamaterial behavior in his early paper. His work was expanded by Pendry et al. 30 years later, when they discovered that a periodically arranged array of thin wires can be used to create an effective negative permittivity material.[4] A year later Pendry et al. published another paper describing the use of micro structured split ring resonator (SRR) arrays to create an artificial effective negative permeability material.[5] As a result, the SRR has become fundamental in metamaterial design.[6,7,8,9,10,11,12,13,14,15,16,17,18,19] Materials fabricated with SRRs have a defined resonant frequency limiting the spectral range at which the structure will exhibit negative values for the effective permeability. The resonant frequency $\left(w_0 \approx (LC)^{-1/2}\right)$ is governed by the geometry of the SRR and is dependent on the self inductance, L, of the metal trace and the capacitance, C, from the gap region of the resonator. For wider bandwidth applications, methods to expand the range that a SRR exhibits an effective negative permeability have become a priority. Tuning of the resonant frequency has been attempted with liquid crystals,[6,7] lumped varactors,[8,9,10,11,12] semiconductors,[13,14,15] and MEMS switches.[16,17,18]

In this paper, we present an approach to monolithically fabricate a MEMS cantilever beam array in the gap region of SRRs to enable electrostatic tuning of the gap capacitance, and thus shift the resonant frequency. This approach was first described in.[19] The *in-situ* fabrication design has several advantages over design methods that utilize varactor diodes such as using less space and eliminating radiation loss from externally wire-bonded components. The *in-situ* fabrication also affords improved yield and scalability due the uniformity of the MEMS-based capacitors.

Device Design
The Split Ring Resonator
The initial SRR geometries were adapted from Smith et al. and then modified to meet the design requirements for the cantilever beams.[20] A schematic of the SRR sans the cantilever array is shown in Fig. 1. The SRR is slightly rectangular with a height of 2400 µm and a width of 2200 µm. The width of the metal trace is 200 µm for both the inner and outer SRR, except for the sides containing the gap which has been expanded to 400 µm to accommodate the array of cantilevers. The inner/outer ring separation is 150 µm and the gap separation begins as 280 µm. The gap region is decreased in a stair step fashion to create identical overlapping areas for each of the varying length beams. The gap is decreased by

25 µm for an overall decrease of 100 µm for the shortest beam. This design feature ensures that each beam will contribute the same amount to the overall capacitance as it actuates.

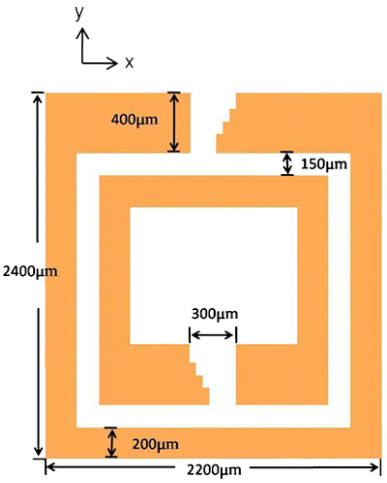

Fig. 1 Schematic of the SRR unit cell showing the modifications to the gap region to accommodate the cantilever

The Cantilever Beam Array

The cantilever beam array was designed to provide a continuous transition of the resonance frequency as the beams actuated or pulled-in. To achieve a steady increase in the resonance a small step increase in the capacitance was desired. This was accomplished by altering the SRR gap region to create identical landing pads for each beam. The beam dimensions were chosen so that upon actuation approximately 2 pF were added to the overall capacitance of the structure. The cantilever array was also designed to actuate at low voltages. To ensure the low voltage requirement the beam dimensions and dielectric were chosen carefully.[21]

The cantilever array consists of 5 beams separated by 10 µm that are 75 µm wide and have lengths of 300, 325, 350, 375, and 400 µm. Figure 2 is a diagram showing the mechanical layer of the cantilever beam array. The beam thickness is 4.75 µm, confirmed through profilometer measurements after the fabrication process. Each beam is fixed to one side of the SRR gap and overlaps the other end of the SRR by 120 µm. The initial gap height of the beams is 2 µm. Beneath each beam is a separate drive electrode that is 120 µm by 75 µm. The electrode is 10 µm away from the edge of the SRR. All the electrodes in the array are electrically connected so that one voltage source can be used to actuate all of the beams.

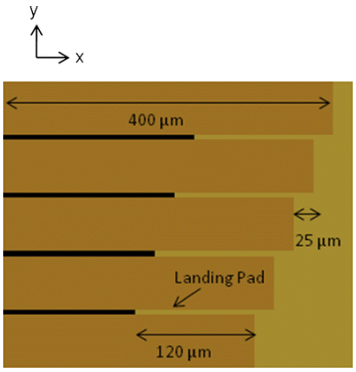

Fig. 2 Diagram of the MEMS cantilever beam array. The cantilever array is located in the gap of both the inner and outer resonators

To achieve the desired added capacitance the landing area of the SRR is coated in a dielectric. Silicon nitride (Si_3N_4) was chosen as the dielectric due to its high dielectric constant (6–9).[22] The Si_3N_4 was deposited using plasma enhanced chemical vapor deposition (PECVD). The dielectric strength of PECVD silicon nitride is 5 MV/cm which corresponds to a breakdown voltage of 150 V for a 3000 Å-thick film,[22] which is well above the range required to pull-in the cantilever beams. PECVD deposited films often exhibit "pin holes" which can reduce the breakdown voltage however, not significantly enough to inhibit beam actuation. Per the pull-in voltage calculations in the next section the breakdown voltage would have to decrease by a factor of 2.5 before the nitride became the limiting factor in the device design.

Calculations and Simulations

In a previous work,[23] a simple equation was used to calculate the pull-in voltage that was also used in[24] to good agreement. However, a more detailed equation is required considering the dielectric layer that is present on the landing pad of the cantilevers. With this layer, the cantilevers in the raised position can be represented as two capacitors in series; one separated by air and the other by a dielectric. When the cantilevers are in the raised position the dominating capacitor will be that with the air gap. As the cantilevers pull-in, the dielectric capacitor will become more dominant. The capacitance between two parallel plates is defined by

$$C = \frac{\varepsilon_0 \varepsilon_r A}{d} \quad (1)$$

where ε_0 is the vacuum permittivity, ε_r is the relative permittivity (air or Si_3N_4), A is the area of the plates and d is the separation distance between the plates. The capacitance of the cantilevers, C_c, is calculated by two capacitors in series.

$$\frac{1}{C_c} = \frac{1}{C_{air}} + \frac{1}{C_{Si_3N_4}} = \frac{C_{air}+C_{Si_3N_4}}{C_{air} \bullet C_{Si_3N_4}} = \frac{\varepsilon_{Si_3N_4}\varepsilon_{air}\epsilon_0 A}{\varepsilon_{Si_3N_4} d + \varepsilon_{air} t} \quad (2)$$

where A is the contact area of the cantilever and the landing pad, d is the initial height of the raised cantilevers, and t is the thickness of the dielectric. As the beams begin to pull-in, changing the value of d has little consequence on the contribution to the capacitance since $\varepsilon_{Si_3N_4} d \gg \varepsilon_{air} t$.[24]

The SRR structure has additional capacitance besides that due to the cantilevers. Capacitance, C_{SRR}, from the SRR gap region and the inner/outer ring separation can be calculated using equation (1). When calculating the overall capacitance the functionality of the array must be considered. As the first beam snaps down, it is now a single capacitor with a separation distance equal to the thickness of the dielectric, and its capacitance, C, can be calculated with equation (1). The capacitance of the remaining beams must still be calculated with equation (2). The beams are in parallel with each other so that the capacitance of each beam is added together to determine the total capacitance. The total capacitance as each beam is pulled-in is given by

$$C_i = C_{SRR} + \sum_{i=0}^{5} (5-i)C_c + iC \quad (3)$$

The calculated capacitances for the SRR gap, inner/outer separation, and the cantilever array are shown in Table 1.

Table 1 The calcualted capacitance values for the SRR and the added capacitance as each cantilever beam is actuated

Capacitance (pF)		**Description**
C_{gap}	0.000048	SRR gap
C_r	0.000050	Inner/outer ring
C_0	0.195	All up
C_1	2.22	4 up, 1 down
C_2	4.26	3 up, 2 down
C_3	6.30	2 up, 3 down
C_4	8.33	1 up, 4 down
C_5	10.36	All down

Equation (2) can be used to derive an expression for the pull-in voltage of the cantilevers. The energy stored in each capacitor is 1/2 C V^2. Setting this equal to the electrostatic force (the derivative of the stored energy as a function of the gap) and solving for the voltage yields

$$V = \left[(d - z) + \frac{\varepsilon_{air}}{\varepsilon_{Si_3N_4}} t\right] \left(\frac{2Nkz}{\varepsilon_{air}\varepsilon_{Si_3N_4}A}\right)^{\frac{1}{2}} \quad (4)$$

where *z* is the movable distance of the cantilever, k is the spring constant, and N is the number of fixtures attached to the plate, for cantilever beams N takes on the value of one. The pull-in distance of the capacitors, determined from equation (4), is found to be

$$z_{pi} = \frac{1}{3}\left(d + \frac{\varepsilon_{air}}{\varepsilon_{Si_3N_4}} t\right) = 670nm \quad (5)$$

The pull-in voltage can be determined by substituting the pull-in distance into equation (4).

$$V_{pi} = \frac{2}{3}\left(d + \frac{\varepsilon_{air}}{\varepsilon_{Si_3N_4}} t\right) \left[\frac{2Nkz}{3\varepsilon_0 A}\left(d + \frac{\varepsilon_{air}}{\varepsilon_{Si_3N_4}} t\right)\right]^{\frac{1}{2}} \quad (6)$$

The pull-in voltages calculated for the cantilever array are given in Table 2. For the above calculation the spring constant was calculated as

Table 2 The calculated pull-in voltages along with pull-in voltages measured using the Zygo for one set of cantilever beams and the entire array of 17 sets of beams

Beam length (µm)	Calculated V_{pi}(V)	Measured (One Set) V_{pi} (V)		Measured (array) V_{pi} (V)	
400	15.5	15	41	30	30
375	17.7	18	50	35	35
350	20.3	20	50	33	45
325	23.5	21	60	40	55
300	27.6	22	70	55	55

$$k = \frac{E'wt_b^3}{2a^2(3L-a)} \quad (7)$$

where E' is the reduced Young's modulus (the Young's modulus weighted by Poisson's ratio) [21] for electroplated gold, w is the width of the beam, t_b is the thickness of the beam, a is the load position of the beam, and L is the length of the beam. The spring constants for the 300, 325, 350, 375, and 400 µm beams were calculated to be 34.7, 20.3, 13.8, 9.8, and 7.3 µN/m, respectively.

The SRR and cantilever designs were modeled with CST Microwave Studio ® (CST MWS), a 3D full wave solver employing the Finite Integral Time Domain and Finite Element Method techniques, to numerically determine the resonance of the fabricated structures.[25] For the simulations an array of 4 SRRs were considered inside a waveguide with a cut-off wavelength of 18 GHz (see Fig. 3). The array is subject to a transverse electromagnetic (TEM) plane wave with open boundary conditions. The fundamental TEM mode excitation is generated by the port on the left of Fig. 3 and propagates to the right. The cantilevers are modeled as lumped capacitive elements with pre-assigned values determined with the above equations and shown in Table 1. CST MWS simulations indicate that a SRR with the above dimensions should display a resonance at 10 GHz, while the SRR with cantilevers should have resonances around 7 and 14 GHz. The dual resonances clearly indicate that the addition of the cantilevers to the SRR has a more dramatic effect than a simple addition to the structures capacitance.

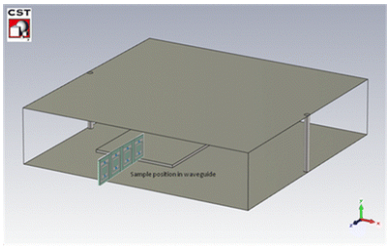

Fig. 3 Diagram of the CST Microwave Studios (MWS) ® 3D model used to simulate the SRR structure in the microstrip waveguide test fixture

Fabrication

The fabrication process used to create the tunable SRR is diagramed in Fig. 4. The structure is built on a 0.5 mm-thick, 3 inch diameter, highly resistive, quartz substrate. First, a base SRR layer is produced by evaporating 5500 Å of gold onto a 200 Å titanium adhesion layer, illustrated in Fig. 4(a). Then a 5500 Å-thick gold electrode was deposited (b), followed by (c) a 3000 Å layer of Si_3N_4 deposited using PECVD. The nitride layer is patterned and then etched with reactive ion etching. After the removal of the unwanted nitride, PMGI is deposited to form a 2 µm-thick beam gap (d). After which, the anchor area is patterned using a deep UV light source (e), followed by a 270°C hot plate bake to reflow the PMGI for the hinges (f). The structural layer is formed by sputtering a thin layer of gold to form a seed layer (g) and then electroplating approximately 5 µm of gold (h). Finally, the PMGI sacrificial layer is removed with 1165 stripper to release the cantilevers (i). The removal is followed by four isopropyl and methanol baths and then dried in a CO_2 critical point dryer.

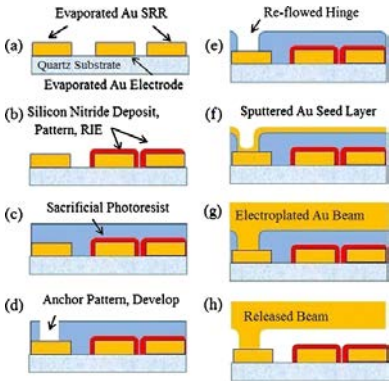

Fig. 4 Annotated fabrication process used to produce the SRR with the MEMS canilever beam array in the gap regions

Gold was chosen for the SRR and cantilever structures because it can also be easily electroplated, deposits with low stress when electroplated, and is conductive. Initially, the electroplated cantilever beams curled upward following the release process (as seen in Fig. 5(a)) indicating that a residual tensile stress was present in the electroplated gold mechanical layer. The electroplated area was then expanded to cover not only the cantilevers but also the entire SRR. Increasing the overall electroplated area reduced the residual stress of the beams and allowed them to lay flat as shown in Fig. 5(b). This improvement to the fabrication process ensured that the as-fabricated devices (i.e. flat beams) closely matched the parallel plate capacitor model used for the initial designs.

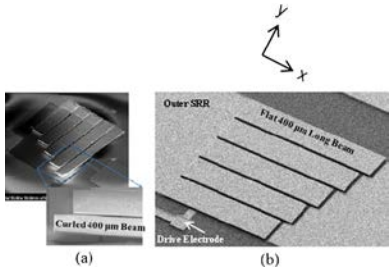

Fig. 5 (**a**) Electroplated cantilevers curled up due to residual stress in the electroplated gold layer and (**b**) the flat beams that resulsted after changing the fabrication process to electroplate both the cantilevers and the SRR

Increasing the electroplating area fixed the beam curling problem however; it also caused the voltage line that connects the inner cantilevers to short to the outer SRR. Two methods were devised for removing the short. Method one consisted of using a focused ion beam (FIB) to separate the voltage line from the SRR, as shown in Fig. 6(a). The second method used a FIB to cut the voltage line on either side of the outer SRR as shown in Fig. 6(b). Making these cuts had several effects on the overall structure.

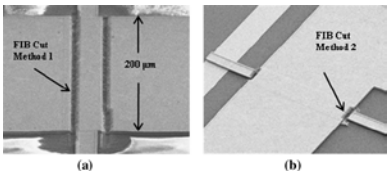

Fig. 6 (**a**) FIB cut 1 cuts the outer SRR to eliminate the shorted voltage line and reders the outer cantilevers inoperable while (**b**) FIB cut 2 cuts the voltage line and removes the functionallity of the cantilevers on the inner SRR

The samples prepared with FIB cut 1 (described above as method one) do not have working outer cantilevers. The two 5 µm slits made to the outer SRR sever the connection between the ground and the outer cantilevers. The outer cantilever actuation pads are still connected to the voltage line but the cantilevers no longer connect to the ground and can therefore not be actuated. Additionally, FIB cut 1 introduces a new source of capacitance causes due to the new gap regions that was not accounted for int eh initial calculations. CST MWS simulations indicate that the SRR with the FIB cuts on the outer ring will have a resonance around 12.5 GHz, which is slightly lower that the 14 GHz predicted for the intact structure. FIB cut 2 (described above in method 2) splices the voltage line that is used to actuate the inner cantilevers while leaving the outer SRR intact. This cut renders the inner cantilevers inoperable but does not changes the results of the initial CST MWS simulations.

Testing

Samples were prepared into strips containing one row of 17 SRRs with contact pads at one end. The 17 cantilever arrays on the inner and outer SRRs were inspected prior to testing. It was observed that a few of the cantilever beams were stuck down. Different cleaning techniques were employed to remedy the beam stiction problem; however it was impossible to eliminate it completely. The beams were observed to actuate with an applied voltage and to return to their original position as the voltages was decreased back to zero.

The DC testing to ensure the cantilevers actuated and to determine the actuation voltages of the beams was accomplished with a Zygo White Light Interferometer. The Zygo clearly indicates when the beams have pulled-in. The cantilevers were monitored with the Zygo while the voltage was increased in even steps to accurately determine the pull-in voltages of the individual beams. The measured pull-in voltages, provided in Table 2, closely match the calculated pull-in voltages for individual sets of beams. Minor differences in the measured and analytic voltages are attributed to differences in actual geometries and thin film properties of the as fabricated devices. While the FIB cuts did not affect the pull-in voltages for the individual sets of beams, the measure pull-in voltages for the arrayed system were approximately two times greater than predicted. This discrepancy resulted when a resistive channel, sufficient to drop the voltage difference between measured and predicted values, formed during the FIB milling. The samples with FIB cut 2 shorted at 35 applied volts so that only the two longest beams could be actuated. As the voltage was applied to the arrayed system, actuation of

cantilevers on the first, eighth, and sixteenth inner SRRs were observed. The pull-in voltages for different arrayed samples are also recorded in Table 2, along with the calculated pull-in voltages. The variation in the measured voltages from sample to sample is mainly due to slight differences in the thickness of the beams from the electroplating process.

Following the DC testing the samples were placed in a microwave strip line to measure the S-parameters of the structure. The strip line was calibrated, however gating was not completed resulting in noisy measurements. Figure 7 shows the resonant frequency for an array of SRRs with FIB cut 1 as the applied voltage is increased from 0 to 60 V, actuating the cantilevers. For clarity the resonance around 14 GHz is expanded and shown in the inset. These samples show dual resonant frequencies at 7.3 and 14.2 GHz however, tuning is only evident on the 14.2 GHz resonance. As the applied voltage is increased to 10 and 20 V (not shown) there is no shift in the resonant frequency which corresponds to the onset of the actuation of the beams at 30 V. Increasing the applied voltage to 30 volts, actuating the 400 µm beams and often the 375 µm beams in close succession caused the resonance to shift about 0.54 GHz to 13.68 GHz. The frequency shifts 1.6 GHz when all the cantilevers are actuated; since each beam contributes the same amount to the capacitance the resonance frequency should shift approximately 0.3 GHz as each cantilever is actuated. At 30 V, the shift is 0.54 GHz indicating that the 400 µm beams pull-in and many of the 375 µm beams may also have actuated. As the voltage is further increased to 40 volts, the frequency shifts only 0.06 GHz to 13.62 GHz. This voltage is representative of the average actuation voltage for the second beam. However, the first and second beam often actuated together, which explains the large initial shift followed by a smaller shift. As the voltage is increased to 45 V, the resonant frequency shifts 0.12 GHz to 13.5 GHz indicating that about half of the 350 µm beams actuated. Further increasing the voltage to 55 V causes the resonance to become 13.14 GHz for an overall shift of 0.36 GHz. At 60 V, all the beams should be actuated. The resonant frequency is 12.66 GHz, a 0.48 GHz shift from the previous voltage, for an overall shift of 1.6 GHz. Although there is some non-uniformity in the cantilever beams, the resonance still exhibits a smooth almost continuous shift over a 1.6 GHz range. The resonance shifts to 12.6 GHz at 60 applied volts, corresponding to the actuation of all the cantilevers and an additional 10.4 pF of capacitance.

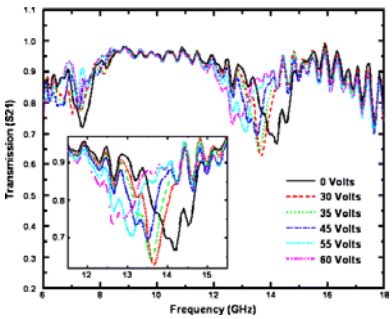

Fig. 7 Transmission from a 1 × 17 array of the cantilever embedded SRR structures with FIB cut 1. As the applied voltage is increased the resonant frequency shifts from 14.2 GHz to 12.6 GHz

Each sample also displays a small resonance at 7.3 GHz that does not shift with the actuation of the cantilevers. The resonance is an artifact of the cantilevers on the outer ring not actuating due to the FIB cut. It is not present in the CST simulations for the original SRR structure, but does appear in the simulations that include FIB cut 1 to the outer SRR.

Figure 8 shows the measured data for the samples with FIB cut 1 at 0 and 60 volts applied overlaid with the simulation data for all the cantilevers raised, C_0 , and all the cantilevers pulled-in, C_5 . The simulation indicates that the SRR should initially have two resonances, one around 7 GHz and the other around 12.6 GHz; however, when all the cantilevers are pulled-in the 7 GHz resonance disappears. Both resonances are measured from the physical structure and the 7 GHz resonance is still present with 60 applied volts. When no voltage is applied the measured resonance is 14.2 GHz, not the 12.6 GHz indicated by the CST MWS simulations. This difference is most likely a result of using lumped elements for the cantilevers in the simulations. The simulated data also shows a considerably smaller shift in the resonance with the additional capacitance from the cantilevers. In general, the simulations do an adequate job of predicting device performance of the cantilever embedded SRRs.

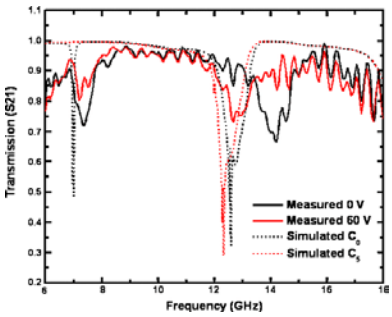

Fig. 8 CST MWS ® simulations (dashed lines) of the SRR embedded with MEMS structres with FIB cut 1 for the (C_0) cantilevers all raised and (C_5) the cantilevers all pulled-in. The simulations are overlaid with the corresponding measured data (solid lines) at 0 and 60 volts

The measured transmission data for the samples with FIB cut 2 to the voltage line are shown in Fig. 9. These samples show a considerably weaker signal than the samples with FIB cut 1. The resonant frequencies are also slightly shifted to 8.4 and 13.5 GHz as compared to the samples with FIB cut 1.For this sample set the outer cantilevers are actuating the resonant frequency around 8 GHz experiences a slight shift at the voltage is increased from 0 to 34 V. As mentioned previously, the samples with FIB cut 2 short if the applied voltage is greater than 35 V, which limited testing to the actuation of the 400 and possibly the 375 µm beams. Thermal images of the samples indicate the short occurs along the voltage lines. With no applied voltage the samples display a resonance at 8.4 GHz. At 26 V, the resonant frequency shifts 0.03 GHz, this minor shift is attributed to a slight decrease in the air capacitor as the beams begin to actuate on the outer SRR. Further increasing the voltage to 30 V, the resonance shifts 0.12 GHz, as the 400 µm beam actuates. When the applied voltage is increased to 34 V, the resonant frequency is 8.0 GHz, for an overall shift of 0.34 GHz, which is attributed to the actuation of the 400 µm beams and partial actuation of the 375 µm beams. The frequency shift for samples with FIB cut 2 are much smaller than those with FIB cut 1. This may be attributed to the different effects the added capacitance will have on the inner/outer SRRs due to their size difference. The samples with FIB cut 2 also have a resonance at 13.5 GHz that does not tune as the cantilevers are actuated.

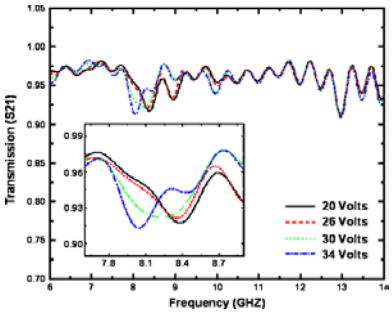

Fig. 9 Transmission from a 1 × 17 array of the cantilever embedded SRR structures with FIB cut 2. As the applied voltage is increased the resonant frequency shifts from 8.4 GHz to 8.04 GHz

Conclusion

Split ring resonators fabricated with MEMS cantilever beams in the gap were fabricated to enable electrostatic tuning of the resonant frequency. A short in the initial design allowed for individual testing of the inner and outer SRRs. The fabricated structures exhibit dual resonances at 7.3 and 14.2 GHz for the inner SRR and 8.4 and 13.5 GHz for the outer SRR. As the cantilever beams actuate on the outer SRR the higher frequency smoothly shifts from 14.2 to 12.6 GHz while the lower frequency remains constant. In contrast, when the 400 and 375 μm beam on the inner SRR actuated the higher resonant frequency of 13.5 GHz remained constant while the 8.4 GHz frequency shifted to 8.0 GHz. The cantilever beams actuated in order of length although there is an element of non-uniformity along the 1×17 array. The fabrication process produced flat beams that pull-in as designed with threshold voltages of 30–60 V. The resonance data is supported with CST MWS simulations.

Notes

Acknowledgements

The financial support and sponsorship of this project were provided by Drs. Katie Thorp and Augustine Urbas from the Air Force Research Laboratory (AFRL), Material and Manufacturing Directorate. The authors are also thankful to the AFRL, Sensors Directorate for assistance and advice during device fabrication.

References

1. Pendry JB (2000) Negative refraction makes a perfect lens. Phys Rev Lett 85:3966–3969
2. Pendry JB, Schrig D, Smith DR (2006) Controlling electromagnetic fields. Science 312:17801782
3. Veselago VG (1968) The electrodynamics of substances with simultaneously negative values of ε and μ. Sov Phys Usp 10:509–514
4. Pendry JB, Holden AJ, Robbins DJ, Stewart WJ (1998) Low frequency plasmons in thin wire structures. J Phys Condens Matter 10:4785–4809
5. Pendry JB, Holden AJ, Robbins DJ, Stewart WJ (1999) Magnetism from conductors and enhanced non linear phenomena. IEEE Trans Microwave Theor Tech 47:2075–2084
6. Ekemkci E, Turhan-Sayan G (2009) Comparative investigation of resonance characteristics and electrical size of the double-sided SRR, BC-SRR, and conventional SRR type metamaterials for varying substrate parameters. Prog Elertomagn Res B 12:35–62

7. Zhao Q, Kang L, Du B, Li B, Zhou J, Tang H, Liang X, Zhang B (2007) Electrically tunable negative permeability metamaterials based on nematic liquid crystals. Appl Phys Lett 90:011112Xiao S, Chettiar U, Klidshev A, Drachev V, Khoo IC, Shalaev V (2009) Tunable magnetic response of metamaterials. Appl Phys Lett 95:033115
8. Reynet O, Acher O (2004) Voltage controlled metamaterial. Appl Phys Lett 84:1198–1200Gil I, Bonache J, Garcia-Garcia J, Martin F (2006) Tunable metamaterial transmission lines based on varactor-loaded split-ring resonators. IEEE Trans Microwave Theor Tech 54:2665–2674Chen H, Wu B, Ran L, Grzegorczyk TM, Kong JA (2006) Controllable left-handed metamaterial and its application to a steerable antenna. Appl Phys Lett 89:053509
9. Aydin K, Ozbay E (2007) Capacitor-loaded split ring resonators as tunable metamaterial components. J Appl Phys 101:024911
10. Gil M, Damm C, Giere A, Sazegar M, Bonache J, Jakoby R, Martin F (2009) Electrically tunable split ring resonators at microwave frequencies based on barium-strontium-titanate thick films. Eletron Lett 45:417–418
11. Chen HT, O'Hara JF, Azad AK, Taylor AJ, Averitt RD, Shrekenhamer D, Padilla WJ (2008) Experimental demonstration of frequency-agile terahertz metamaterials. Nat Photonics 2:295–298Boulais KA, Rule DW, Simmons S, Santiago F, Gehman V, Long K, Rayms-Keller A (2008) Tunable split-ring resonator for metamaterials using photocapacitance of semi-insulating GaAs. Appl Phys Lett 93:043518
12. Han J, Lakhtakia A, Qui CW (2008) Terahertz metamaterials with semiconductor split-ring resonators for magnetostatic tunability. Opt Express 16:14390
13. Gil I, Martin F, Rottenberg X, De Raedt W (2007) Tunable stop-band filter at Q-band based on RF-MEMS metamaterials. Electron Lett 43:1153–1154
14. Hand T, Cummer S (2007) Characterization of tunable metamaterial elements using MEMS switches. IEEE Antennas Wirel Propag Lett 6:401–404
15. Langley D, Coutu RA, Starman LA (2010) MEMS integrated metamaterial structure capable of variable resonance for RF applications. 11th International Symposium MEMS and Nanotechnology. SEM Annual Conference, Indianapolis, IN, 7–10 June
16. Smith D, Vier DC, Koschny T, Soukoulis CM (2005) Electromagnetic parameter retrieval from inhomogeneous metamaterials. Phys Rev E 71:036617
17. Finot E, Passian A, Thundat T (2008) Measurement of mechanical properties of cantilever shaped materials. Sensors 8(5):3497–3541
18. Madou M (1997) Fundamentals of microfabrication. CRC, New York, p 300
19. Coutu RA Jr, Collins PJ, Moore EA, Langley D, Jussaume ME, Starman LA (2011) Electrostatically tunable meta-atoms integrated with *in-situ* fabricated MEMS cantilever beam arrays. Submitted to the IEEE/ASME J MEMS, Submitted Sept 10, revised and resubmitted Feb 11
20. Lou JK, Lin M, Fu YQ, Wang L, Flewitt AJ, Spearing SM, Fleck NA, Milne WI (2006) MEMS based digital variable capacitors with high-k dielectric insulator. Sens Actuators A 132:139–146